Digest 2017, December 2017, 2079-2096

On the Use of Shallow Water Equations in Hydraulics†

Behiye Nilay İŞCEN[1]
Nuray ÖKTEM[2]
Burak YILMAZ[3]
İsmail AYDIN[4]

ABSTRACT

Shallow water equations are widely used in inundation analysis as they are known to be successful in computation of flood inundations over wide terrains. Flood propagation in between buildings in urban areas and flows around hydraulic structures such as bridges may not satisfy the assumptions of shallow flow and may display markedly more 3-Dimensional (3D) flow characteristics. However, shallow flow equations can be used for such 3D flows also to allow fast numerical solution and a useful output may be obtained.

In this study, shallow water equations are applied to flows with prominent 3D characteristics and results are evaluated. Water depths and velocity field in horizontal plane were calculated satisfactorily, surface waves in supercritical flow involving shocks were described in detail. However, in flows passing around more than one obstruction, there is a cumulative increase in error in the computed water depths. In case of uniform flows with boundary layer characteristics, velocity and bed shear stresses were predicted successfully using a suitable turbulence model.

Keywords*: Flood, flood inundation, shallow water equations, shock capturing solutions, Riemann solvers.*

1. INTRODUCTION

In hydraulic engineering applications involving free surface flows, water depth calculation is a first step in making detailed analysis of flow conditions. To this end, the numerical solution of 1D integral equations is a common application and used in river engineering computations since the second half of the 20th century. One dimensional solutions which became much easier with the development of computers, have been used to compute the propagation of inundation waves especially in dam-break type problems.

Although the flows in natural environment are always 3D one can take the advantage of simplified 1D or 2D mathematical models in order to achieve practical and quick solutions for engineering applications. Today, 3D comprehensive numerical solutions can only be achieved in limited size flow domains such as flow around important hydraulic structures

1 Middle East Technical University, Ankara, Turkey - bnilayiscen@gmail.com
2 Çanakkale Onsekiz Mart University, Çanakkale, Turkey - nbozkaya@gmail.com
3 Middle East Technical University, Ankara, Turkey
4 Middle East Technical University, Ankara, Turkey - ismaydin@metu.edu.tr

† Published in Teknik Dergi Vol. 28, No. 1 January 2017, pp: 7747-7764

like spillways, stilling basins and bridges. 3D solutions for flood areas and the river beds extending tens of kilometers are not economic and not required. Time accurate solutions have to be made to compute the flow propagation for the purpose of flood analysis. However, since the variation of flow parameters in vertical direction is not necessary for flood analysis, it is sufficient to solve the equations for the depth averaged values obtained by integrating the governing equations over the flow depth. In this case, the continuity equation is solved for the flow depth and the two momentum equations in horizontal directions are solved for the depth averaged horizontal velocity components. The depth integrated flow equations are called 'Shallow Water Equations' (SWE) and they are used not only for flood analysis but also for lakes, wave propagation in coastal areas, currents and circulation in the ocean, and flows in the layers of the atmosphere. The basic condition for the validity of the SWE is that the horizontal dimensions have to be significantly larger than the vertical dimension.

If SWE is used for a free surface flow, significant advantages are achieved in the numerical solution process. The continuity equation is solved for the water depth, the problem of determining the water surface location in 3D numerical solutions is thus unnecessary. In addition, since the vertical acceleration is ignored during the depth integration, hydrostatic pressure distribution is assumed. Therefore, there is no need to solve an equation for pressure in SWE formulation. As a cost of such dramatic simplifications in mathematical modeling and numerical solution, SWE incur significant physical restrictions in their use for different flow problems. In this study, it is aimed to discuss limitations of SWE applied to some hydraulic problems.

2. SHALLOW WATER EQUATIONS (SWE)

The SWE system, based on integration of the Navier-Stokes equations in the vertical direction [1], consists of the continuity and two horizontal momentum equations. Vector notation will be used in order to present a compact form of the system of equations and its numerical solution.

$$\frac{\partial \boldsymbol{U}}{\partial t} + \nabla \cdot \boldsymbol{F^c} = \boldsymbol{S} + \nabla \cdot \boldsymbol{F}^d \tag{1}$$

Here, t is time, $\boldsymbol{U}$ is the vector of dependent variables, $\boldsymbol{F^c} = (E^c, G^c)$ is convective flux, $\boldsymbol{F^d} = (E^d, G^d)$ is diffusive flux, ∇ is the divergence and $\boldsymbol{S}$ is the source vector. Explicit definitions of all these vectors are given in Equation (2)

$$\boldsymbol{U} = \begin{bmatrix} h \\ hu \\ hv \end{bmatrix} \quad , \quad E^c = \begin{bmatrix} hu \\ hu^2 + \frac{1}{2}gh^2 \\ huv \end{bmatrix}, \quad G^c = \begin{bmatrix} hv \\ huv \\ hv^2 + \frac{1}{2}gh^2 \end{bmatrix}, \quad E^d = \begin{bmatrix} 0 \\ \frac{h}{\rho}\tau_{xx} \\ \frac{h}{\rho}\tau_{xy} \end{bmatrix} \quad ,$$

$$G^d = \begin{bmatrix} 0 \\ \frac{h}{\rho}\tau_{yx} \\ \frac{h}{\rho}\tau_{yy} \end{bmatrix}, \qquad S = \begin{bmatrix} 0 \\ gh(S_{0,x} - S_{f,x}) \\ gh(S_{0,y} - S_{f,y}) \end{bmatrix} \tag{2}$$

Here, h is the water depth, u and v are depth-averaged velocities, hu and hv are unit discharges in x- and y- directions respectively, g is the acceleration due to gravity, ρ is water density, τ is the sum of viscous and turbulent stresses, S_0 is the bed slope and S_f is the bed friction slope. In Equation (2), pressure terms are nested in the convective terms since it is appropriate for the numerical solution technique. In the computation of friction slope, the common Manning roughness parameter n is used.

$$S_{f,x} = \frac{n^2\, u\sqrt{u^2+v^2}}{h^{4/3}}, \qquad S_{f,y} = \frac{n^2\, v\sqrt{u^2+v^2}}{h^{4/3}} \tag{3}$$

In many SWE solutions the viscous terms and turbulence are often ignored. This is a common assumption especially for dam-break and flood propagation problems. However, in problems where circulation and formation of vortices on horizontal plane become significant, the viscous effects and turbulent stresses are preserved in the solution. Additionally, the viscous terms are necessary mathematically for applying correct (no-slip) boundary conditions and obtaining accurate velocity propagations in the computation of flows closer to the solid boundaries. For a depth integrated model, the total stresses can be written by utilizing the classical turbulent viscosity approach.

$$\tau_{i,j} = (\nu + \nu_t)\left(\frac{\partial u_i}{\partial x_j} + \frac{\partial u_j}{\partial x_i}\right) \tag{4}$$

here, ν is kinematic molecular viscosity and ν_t is kinematic turbulent viscosity.

Successful Computational Fluid Dynamic (CFD) analysis depends on the correct implementation of the boundary conditions of the problem. Boundary conditions affect the numerical convergence and also determines the physical validity of the solution. In the SWE solutions, the types of boundary can be inflow, outflow, solid, symmetry and periodic. For all the boundary types, the required boundary conditions and number of variables change in accordance with the mathematical model used as well as the state of flow which can be either subcritical or supercritical.

3. NUMERICAL SOLUTION

SWE is a nonlinear system of partial differential equations with hyperbolic characteristics. The most important feature of it is the presence of discontinuities in its solution due to the shock waves that may occur on the water surface. The most common example of the discontinuity in the solution is the idealized 1D dam-break problem in which water behind a vertical wall is left free by sudden removal of the wall. At that moment, the water surface slope at the point of wall is infinite. Hydrostatic water, initially parallel to the vertical wall, deforms rapidly and flows until it recovers another hydrostatic configuration. Namely, all phases of flow from initial hydrostatic to final hydrostatic configuration have to be computed. Therefore, the numerical solution method must be capable of capturing the spatial discontinuities of the dependent variables without smoothing and also calculating the time evolution accurately. In the standard finite difference method the derivatives are expressed in terms of nodal values at two or more neighboring grid points. Such approaches do not work properly especially near the discontinuities.

Finite volume methods are more appropriate in solving spatial discontinuities. In the finite volume approach the flow domain is divided into small finite volumes which are called computational cells. In the numerical solution, cell average values of the dependent variables are computed. In every time step, the fluxes at the faces of the cells are computed first and the average value of the dependent variable in the cell center is obtained by integration of the equations over the cell volume. The success of the numerical solution depends on the accurate computation of the surface fluxes even in the case of the discontinuity of the variables.

Hyperbolic partial differential equations describe propagation problems. Many flows in nature show hyperbolic character which is simply described as a wave pattern. In this type of flow, the previous value of a variable at a point can change the flow conditions by affecting a current value at another point. In other words solution at a given point propagates together with the flow. Several schemes are available for the computation of the interface fluxes and the numerical solution strongly depends on the scheme used. The commonly used upwind schemes allow more accurate numerical flux computations since they take account of the direction of the flow while obtaining the interface fluxes.

A one-sided Riemann problem is solved while computing the cell interface fluxes considering that the discontinuity may occur for each variable. Riemann problem is based on the assumption that the right and left approximating values of a dependent variable at any interface of a control cell may be different from each other [2]. In this case the interface flux must be obtained by considering all possible wave formations; shock, rarefaction, contact waves and the interactions of all. This process is a complex sequence of conditions and comparisons and is known as ' Riemann solvers ' in the literature. Although the Riemann problem can be exactly solved, approximate Riemann solvers are also widely used since they require less computational time. Besides, the Riemann problem being identified as 1D, can also be used for the solution of higher dimensional problems with sequential applications in each direction.

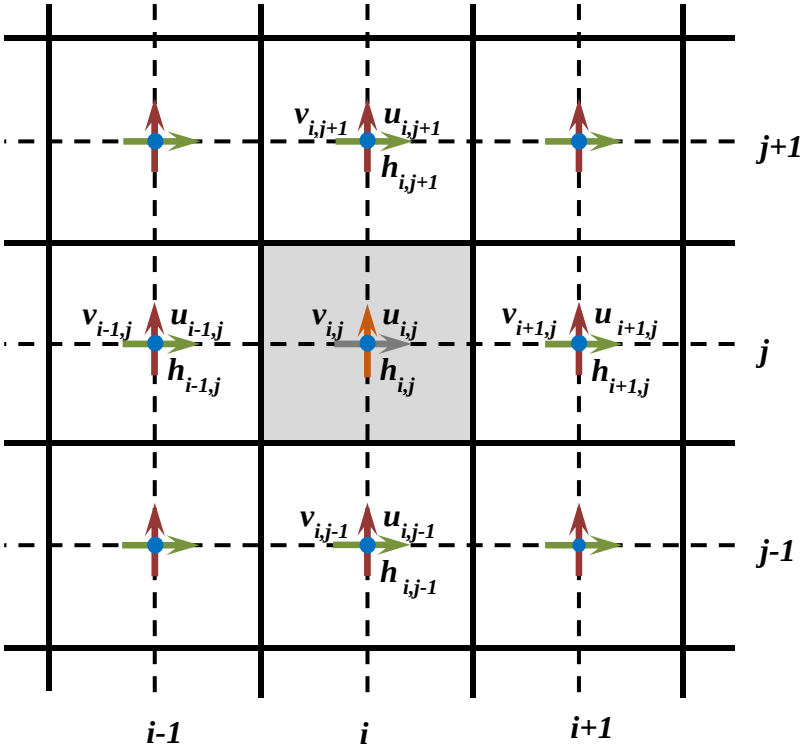

Figure 1. Computational grid and description of dependent variables [3]

When compared with the previous numerical methods, the Godunov method brings a new dimension to CFD applications by benefitting the upwind schemes and Riemann solvers. Basically, the Godunov method aims to obtain the most accurate solution using the first order upwind scheme near the discontinuities involved in the solution of the nonlinear conservation equations. The Riemann solvers whether exact or approximate are basic components of the Godunov method. The method depends on the solution of the Riemann problem at each time step and at all cell interfaces. The finite volume discretization of Equation (1) in a rectangular structured grid (Figure 1) is given in Equation (5).

$$\boldsymbol{U}_{i,j}^{n+1} = \boldsymbol{U}_{i,j}^{n} - \frac{\Delta t}{\Delta x}\left(E_{i+\frac{1}{2},j}^{c}{}^{n} - E_{i-\frac{1}{2},j}^{c}{}^{n}\right) - \frac{\Delta t}{\Delta y}\left(G_{i,j+\frac{1}{2}}^{c}{}^{n} - G_{i,j-\frac{1}{2}}^{c}{}^{n}\right)$$
$$+ \frac{\Delta t}{\Delta x}\left(E_{i+\frac{1}{2},j}^{d}{}^{n} - E_{i-\frac{1}{2},j}^{d}{}^{n}\right) + \frac{\Delta t}{\Delta y}\left(G_{i,j+\frac{1}{2}}^{d}{}^{n} - G_{i,j-\frac{1}{2}}^{d}{}^{n}\right) + \Delta t \boldsymbol{S}_{i,j}{}^{n} \quad (5)$$

Here, $\boldsymbol{U}_{i,j}^{n}$ consists of the dependent variables at a control cell, i, j are the cell indices in x- and y- directions, n is the time level, Δt is the time step, Δx and Δy are cell dimensions, $\boldsymbol{F^c}$ and $\boldsymbol{F^d}$ are the total convective and diffusive fluxes respectively on the cell interfaces. When

the convective fluxes are obtained by using the solution of the Riemann problem at interfaces, the finite volume formula in Equation (5) will be second order in space and have the shock capturing property. In order to have a second order solution in time, a two-step second order accurate predictor-corrector approach is used. At first, predictor values are obtained at half-step in time.

$$\boldsymbol{U}_{i,j}^{P} = \boldsymbol{U}_{i,j}^{n} - \frac{\Delta t}{2\,\Delta x}\left(E^{c}{}_{i+\frac{1}{2},j}{}^{n} - E^{c}{}_{i-\frac{1}{2},j}{}^{n}\right) - \frac{\Delta t}{2\,\Delta y}\left(G^{c}{}_{i,j+\frac{1}{2}}{}^{n} - G^{c}{}_{i,j-\frac{1}{2}}{}^{n}\right) + \frac{\Delta t}{2\,\Delta x}\left(E^{d}_{i+\frac{1}{2},j}{}^{n} - E^{d}_{i-\frac{1}{2},j}{}^{n}\right) + \frac{\Delta t}{2\,\Delta y}\left(G^{d}_{i,j+\frac{1}{2}}{}^{n} - G^{d}_{i,j-\frac{1}{2}}{}^{n}\right) + \frac{\Delta t}{2}\,\boldsymbol{S}_{i,j}{}^{n} \tag{6}$$

In Equation (6) the superscript 'P' indicates the predicted values in half-time step. In the second stage, the corrected values are computed at the full time step level $n+1$ as given in Equation (7)

$$\boldsymbol{U}_{i,j}^{n+1} = \boldsymbol{U}_{i,j}^{n} - \frac{\Delta t}{\Delta x}\left(E^{c}{}_{i+\frac{1}{2},j}{}^{P} - E^{c}{}_{i-\frac{1}{2},j}{}^{P}\right) - \frac{\Delta t}{\Delta y}\left(G^{c}{}_{i,j+\frac{1}{2}}{}^{P} - G^{c}{}_{i,j-\frac{1}{2}}{}^{P}\right) + \frac{\Delta t}{\Delta x}\left(E^{d}_{i+\frac{1}{2},j}{}^{n} - E^{d}_{i-\frac{1}{2},j}{}^{n}\right) + \frac{\Delta t}{\Delta y}\left(G^{d}_{i,j+\frac{1}{2}}{}^{n} - G^{d}_{i,j-\frac{1}{2}}{}^{n}\right) + \Delta t\,\boldsymbol{S}_{i,j}{}^{P} \tag{7}$$

Roe approximate Riemann solver is used while calculating the convective fluxes on the control cell interfaces. Many studies are available ([4], [5]) in the literature about the description and the success of this method. Therefore, they will not be repeated in this paper. One other important feature of the numerical solution is the use of slope- or flux-limiters which are necessary in the limitation of the computed flux values. At any point, the slope of a variable can be infinitely large due to discontinuity. In such a case, the resulting slope (or flux) values have to be bounded in order to maintain the computation process. A large number of experiential function having slope limiting property are available in literature. The Superbee, Van Leer, Van Albada and Minmod limiters have been used through this study [6].

For the sequential computation process defined by Equations (6) and (7) to reach a solution consistently, limitations in time step are necessary. In this work, the time step estimation is made by specifying a CFL number in the formula given below.

$$\Delta t = \mathrm{CFL}\,\min\left\{\frac{\Delta x,\ \Delta y}{\left(c + \sqrt{u^2 + v^2}\right)_{i,j}}\right\} \tag{8}$$

where c is celerity ($= \sqrt{gh}$) and the CFL number is fixed 0.5 in all solutions. The above numerical model is encoded in FORTRAN programming language and run for the 1D dam-break test problems first. The results are compared to analytical solutions available in

literature, the performance of the given approach is tested and it is observed that the obtained solutions have similar accuracy with the reported ones by other researchers. Since 1D test solutions regarding the success of the solution method used in this study are published by different researchers in literature ([7], [8], [9]), they are not going to be repeated here. Results of the three different flow configurations considered in the main theme of this study are presented and discussed in detail in the following sections.

4. APPLICATIONS

4.1. Flow Around a Cubic Block in Prismatic Channel

Accurate simulation of flow events in transitions in open channel flows is important to show the success of the numerical solution. Interaction of shock waves in supercritical flows, transitions in contractions due to an obstacle in the channel and hydraulic jumps are typical flow phenomena to be considered as test cases to validate the numerical scheme. In order to investigate such kind of transient flow details, the SWE are solved initially without the viscous and turbulence terms as in many applications available in literature.

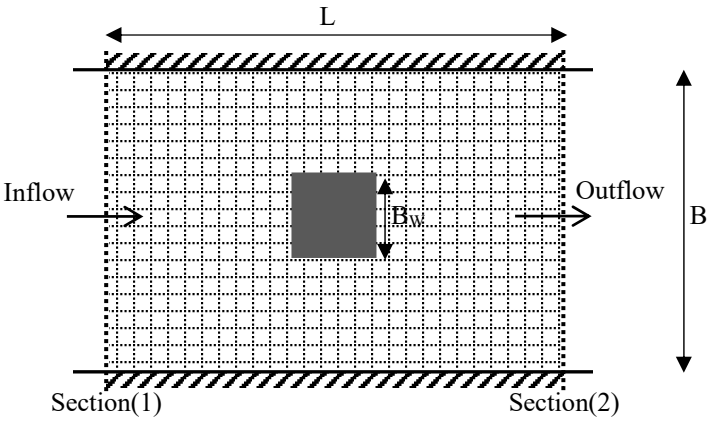

Figure 2. Numerical solution domain of the flow around a cubic block [3]

Flow around a cubic obstacle in a prismatic channel (Figure 2) is examined. On the wall boundaries, non-viscous slip boundary conditions are applied to be consistent with the governing equations in the numerical solution. Since the flow is expected to be symmetric around the block, computations are carried on half of the domain by defining a symmetry boundary condition along the centerline of the channel. On all solid boundaries the normal velocity components are defined as zero while the tangential velocities are allowed to be nonzero implying slip-boundary conditions. On the symmetry axis, the normal velocity is defined as zero to satisfy the no-mass transfer condition. Boundary conditions for the inflow and outflow boundaries are dependent on the flow regime [10]. In the subcritical flow case in the downstream the outflow depth is fixed while in the upstream the inflow unit discharge in both directions is assumed to be constant. Additionally, in the supercritical flow case, in

the upstream the inflow depth and the unit discharges in both directions are fixed and in the downstream the gradients of all dependent variables are set to zero. The velocity components are obtained from the computed unit discharge and depth values in all steps.

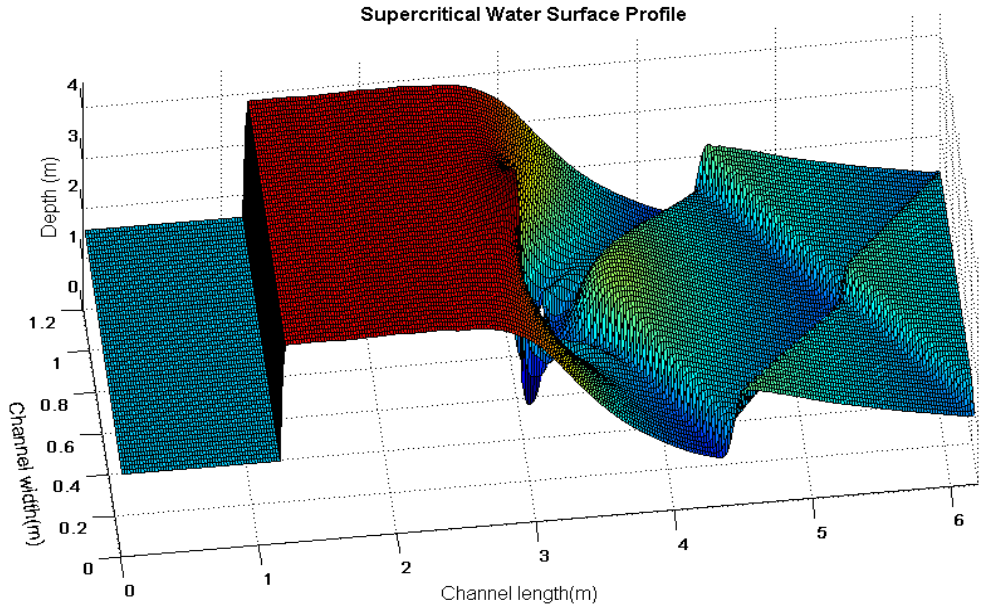

Figure 3. Water surface profile of the supercritical flow around the cubic block [3]

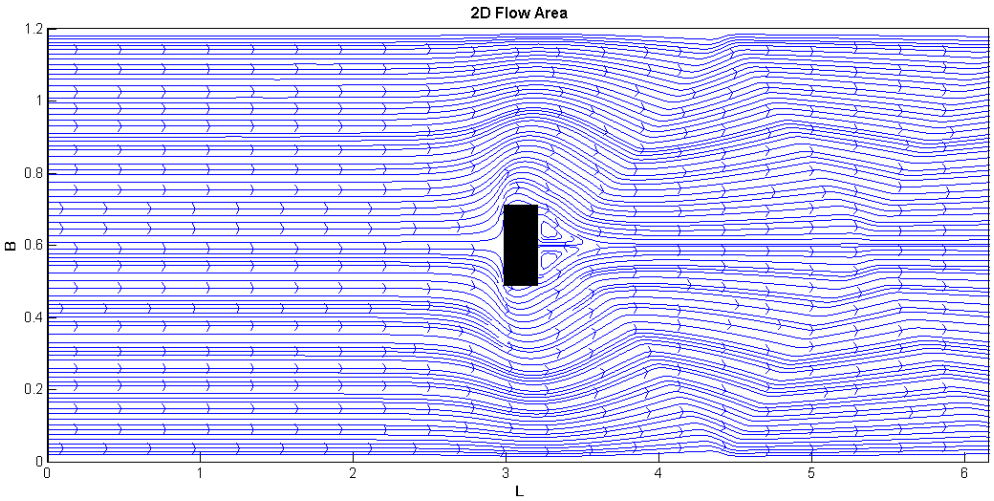

Figure 4. Streamlines in the horizontal plane of the supercritical flow around a cubic block [3]

The numerical solution grid is formed with square cells with constant dimensions. Three different mesh sizes were considered to obtain grid independent solutions. It is observed that all mesh sizes give the same solution and results of the medium mesh are presented. The computational grid involves 60×310 cells. For the supercritical flow case the water surface profile is visualized in Figure 3. The cubic block was fixed in the channel at x = 3 m and its place in the figure is left empty so that the waves occurring on the water surface around the cubic block can be seen. For the given flow conditions, the flow around the block first chocks due to insufficient flow energy and then transitions to the subcritical regime in the upstream to gain enough energy. As a result of this change in flow regime hydraulic jump occurs in front of the block.

In the numerical solution, initially the flow depth is assumed to be the supercritical normal depth all over the solution domain. The hydraulic jump starts on the front face of the block due to chocking and moves upstream until reaching the force balance. Although the flow is time independent, the transient solution methodology allows observation of the flow development until steady-state is reached. The water surface profile shown in Figure 3 is before the steady state position so that the hydraulic jump can be seen close to the block. If the solution domain is elongated in the upstream direction, the hydraulic jump moves far upstream from the block until it stabilizes. The applied numerical method reproduces the hydraulic jump almost vertical, cornered shock wave and computes its upstream movement in the channel without any numerical instability. Moreover the diamond–shaped stationary shock waves which appeared after the block and overlap onto each other due to reflection from the walls and keep their position during the entire solution process. These results show that the numerical method can compute any moving or stationary shock waves, hydraulic jump and chocking. Especially, the hydraulic jump that can be computed almost a vertical front proves that the numerical method can reveal the discontinuities of the flow variables as they are without smoothing or dispersing.

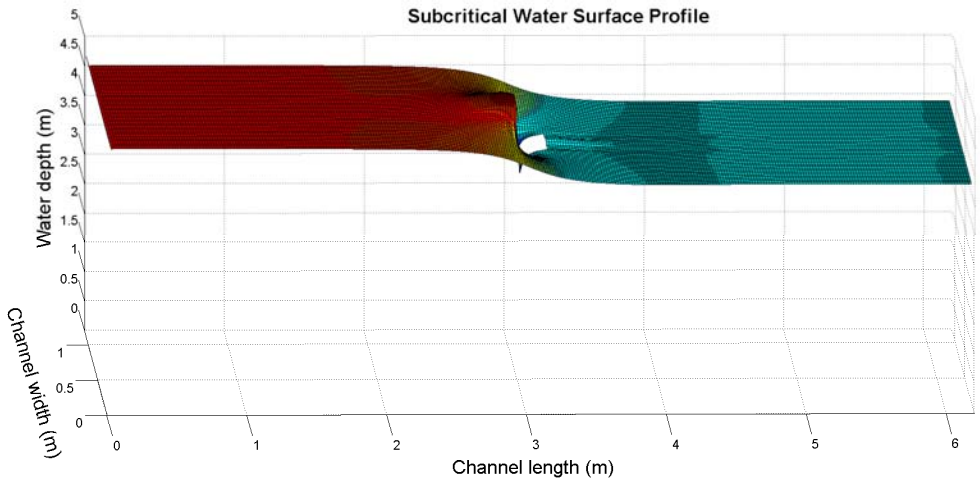

Figure 5. Water surface profile of subcritical flow around a cubic block [3]

The streamlines for the same supercritical flow case are shown in Figure 4. The figure is distorted to make the streamlines more visible. The block at the middle should be viewed as a square. The two vortices at the downstream face of the block and the crossing of the shock waves reflected from the walls can be observed.

A similar numerical solution is obtained for the subcritical flow and the resulting water surface profile is given in Figure 5. Since the flow is subcritical, the water depth increases in the upper face of the block to provide the energy necessary for the flow to pass through the contracted sections around the block. Unlike the supercritical case, no shock wave is formed and the flow pass through around the block by acceleration due to the energy stored in the upstream side.

4.2. Flow in a Prismatic Channel Involving Offset Spur Dikes

The second flow configuration is a channel flow through obstructions. Numerical results of this section is supported by experimental data obtained from a physical model. The 3D flow passing through successive spur dikes arranged in a staggered manner on both walls of a horizontal prismatic channel (Figure 6) is examined [11]. Water accelerates among the dikes with decreased depth and large vortices are developed in the wake of each dike. The interactions caused by a number of large vortices and the associated turbulence highlight the 3D future of the flow. Therefore, the purpose of this test case is to illustrate the SWE solutions for a strongly 3D problem. In such a case, although the SWE solution will be inefficacious for the velocity distributions, the validity of the computed water surface profile is still an arguable output. In fact, it is also known that in some 3D solutions the water surface profile was obtained from SWE solutions.

In the physical model, water surface profiles are measured for different discharges and outflow conditions and then compared with the SWE solutions. Since the flow is turbulent due to vortex motions in it, it was difficult to read water surface elevations due to large fluctuations. The maximum, minimum and average values were determined after 2 minutes of observations at all measurement points. At the end of the channel controlled and uncontrolled outflow cases were tested. In this paper the experimental results only for the uncontrolled outflow cases are compared with the newly obtained numerical SWE solutions. The other cases yield similar results.

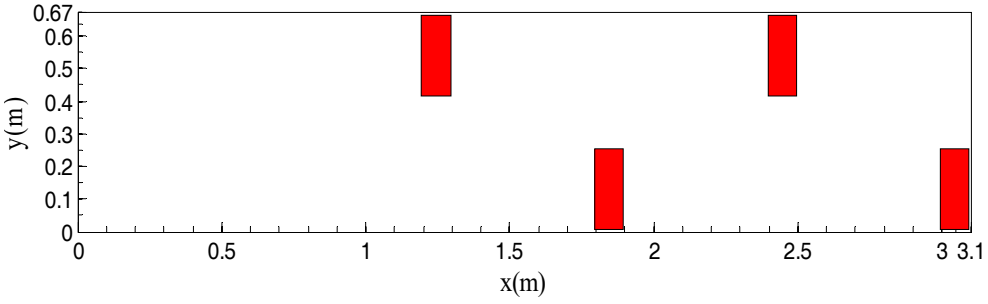

Figure 6. Flow region in a prismatic horizontal channel with staggered spur dikes [11]

In the numerical solution, the viscous terms in Equation (2) are included in order to satisfy the no-slip wall boundary condition and the turbulent stress terms given as in Equation (4) are also added in the computation. The depth integrated value of the turbulence viscosity was fixed for the whole flow area as 0.007 m^2/s after some numerical experiments. In this problem the turbulence viscosity was fixed since there will be no comparison of velocity distributions. The initial measures of the inflow depth and the unit discharges are applied as inflow boundary conditions, however at outlet zero gradients for the flow variables are applied. The outflow boundary condition was applied at a section far downstream to avoid any restrictions in the development of upstream flow.

The water surface measurements for the discharge value of 0.06 m^3/s are presented in Figure 7. In the beginning of the channel the flow is subcritical with the rising water level in front of the blocks and it accelerates while passing through the blocks. Therefore, the water depth descends and the flow regime change to supercritical state with increasing Froude number values. Inherently, the vertical velocity component which was neglected in SWE derivation become more pronounced and also the pressure distributions diverge from hydrostatic. The water surface profile from the numerical solution of SWE is visualized in Figure 8. Although both the experimental and numerical results are in accordance with each other throughout the channel, the numerically obtained water surface profile progressively differs from the experimentally measured profile as the cumulative disturbance given by the blocks increasing in the direction of flow. To clarify this observation, the measured maximum and minimum water levels and the computed water depths along the centerline of the flow channel are compared in Figure 9. Especially after 3rd block it is seen that the computed water surface profile cannot catch up with the measured wavy behavior.

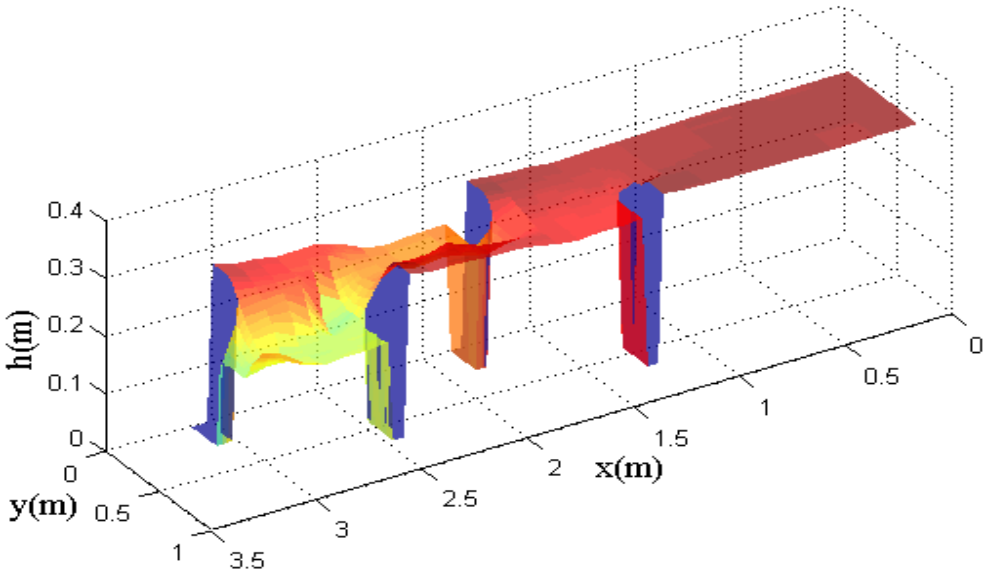

Figure 7. Experimental water surface profile through staggered spur dikes in a horizontal channel[11]

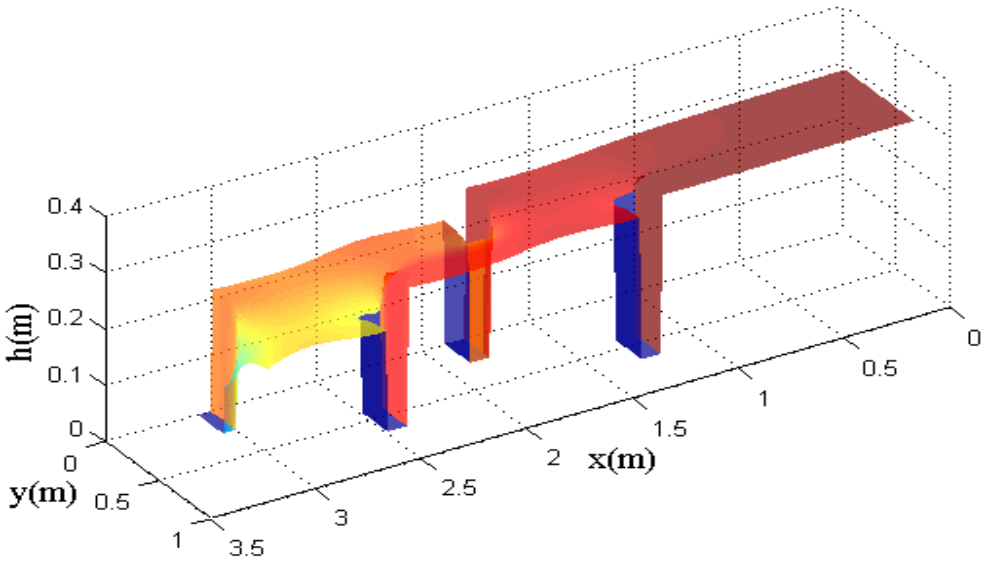

Figure 8. Numerical water surface profile through staggered spur dikes in a horizontal channel

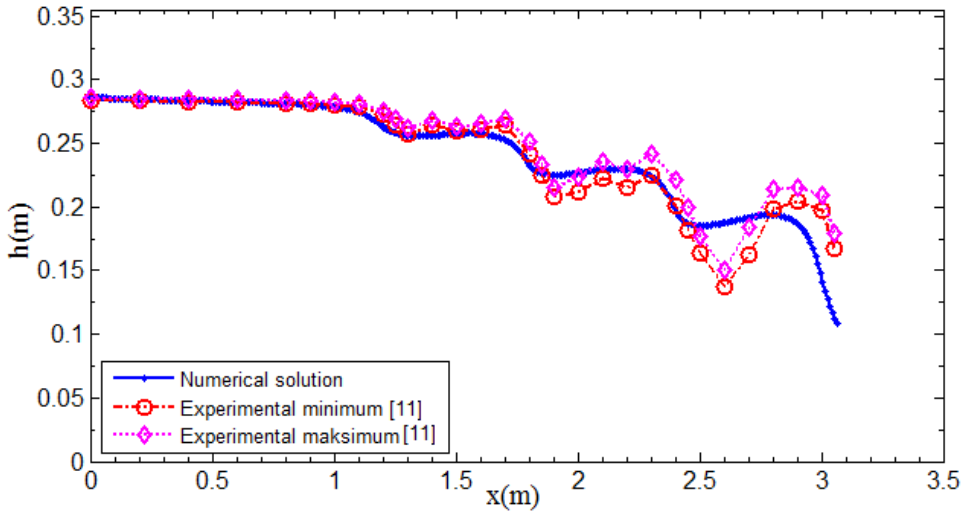

Figure 9. Comparison of experimental and numerical water surface profiles along the centerline of the channel

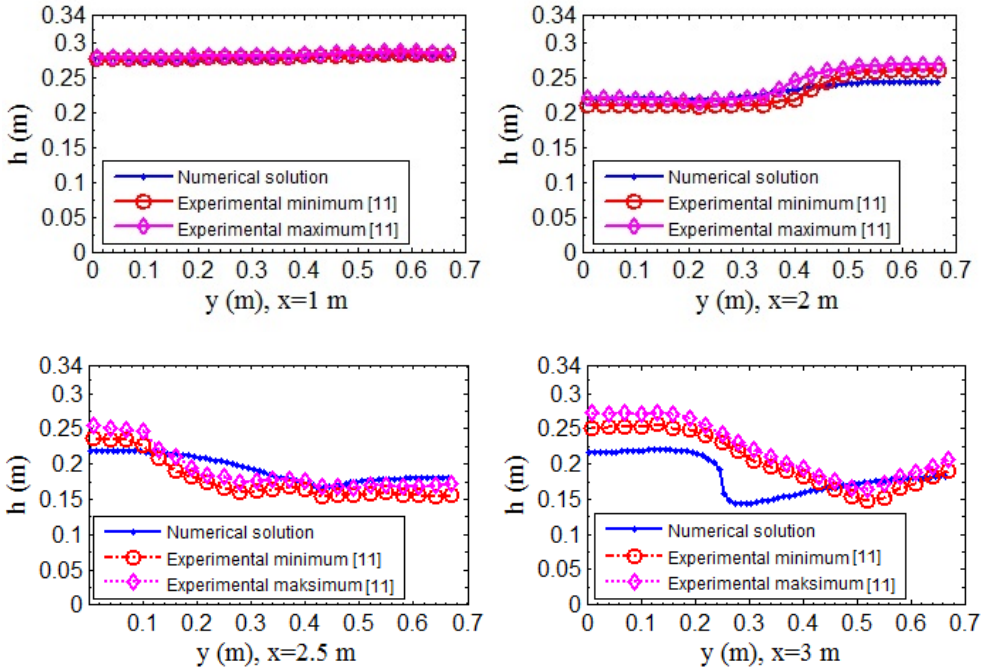

Figure 10. Comparison of experimental and numerical lateral water surface profiles on fixed channel sections

To clarify this observation the experimentally measured and numerically computed water depths along some channel cross-sections are illustrated in Figure 10. Just before the first dike ($x = 1$ m) the calculated and measured values coincide exactly. Immediately after the second dike ($x = 2$ m) a differentiation is observed opposite to the block. After the third dike ($x = 2.5$ m) deviations start to rise and after the fourth dike ($x = 3$ m) the calculated water surface profile and the experimental measures differ considerably. The continuity equation naturally provides exact conservation of the volume along the channel. However, the water volumes thrown laterally among the dikes with increasing acceleration in vertical and the SWE solution is unable to conserve the momentum in the channel.

The streamlines obtained from the numerically calculated depth-averaged velocity are given in Figure 11. It is observed from this figure that large vortex structures are reproduced apparently after the blocks in the horizontal plane. On the other hand it is known that there are also vortices in the vertical planes close to the channel base and the SWE solution is insensitive to these vortices.

Regarding above observations one can conclude that the SWE solutions will be able to give quite accurate results without being affected too much from the 3-dimensionality caused by a single obstruction in the channel. However, by the increasing number of obstructions contributing to the 3-dimensionality, a progressing differentiation occurs between the SWE

solution and the real flow behavior and eventually the difference between the calculated and real values of water depth increases.

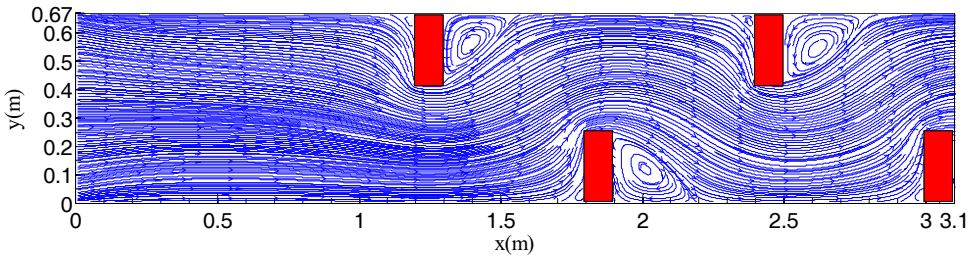

Figure 11. Streamlines obtained from depth-averaged velocity components

4.3. Uniform Flow in a Prismatic Composite Cross Sectional Channel

In the first example above all the viscous terms were neglected. In the second example the viscous terms were included in the computation but the turbulent viscosity was kept constant for the whole flow region. In open channel flows for the correct computation of velocity profiles the turbulent structure must be modelled exactly. In this sense, although there are many studies ([12], [13], [14], [15], [16]) available, yet there is not a generally accepted depth-averaged turbulence model for the SWE modeling. As to some studies rather than defining a model, it is tested to be compatible by experimental data with some empirical expressions [17]. The difficulty here is that the degrading of 3-dimensional turbulence into 2-dimensions conflicts with the basic turbulence mechanisms such as vortex formations.

Open channel flow is an internal flow bounded by the channel walls and the free surface characterized by development of boundary layers. Turbulence at a point in the flow simply depends on the weighted distance from the walls bounding the flow. In general the SWE is insensitive to third dimension of the flow that is the variations in depth. Thus, if the turbulence will be modelled in SWE solution, the most required data is the bounding wall distances or the definition of a mixing length for turbulence. This description should be able to represent the information about the 3D environment in which flow is taking place. In this context, for the uniform flow in prismatic channels, a previously proposed formulation [18] will be used. In this study, firstly the flow is supposed to be uniform and therefore there is no change in the variables in the main flow direction, x. But in the cross section all the three flow components are computed. Although the flow is uniform, turbulence driven secondary flows develop in the corners due to the turbulence un-isotropy. In a cross section perpendicular to the flow direction counter rotating vortices originate and affect the mainstream velocity distribution significantly. Therefore, turbulence driven secondary flows are also computed by the solution of the transverse momentum equations. The model described in the aforementioned study [18], defines a 'turbulence mixing length' referring to the 3-dimensionality of the channel geometry and builds a relationship between the turbulent stresses and the nonlinear correlations of the strain rates. Thus, the secondary flows and the redistribution of the momentum due to secondary flows can be computed accurately.

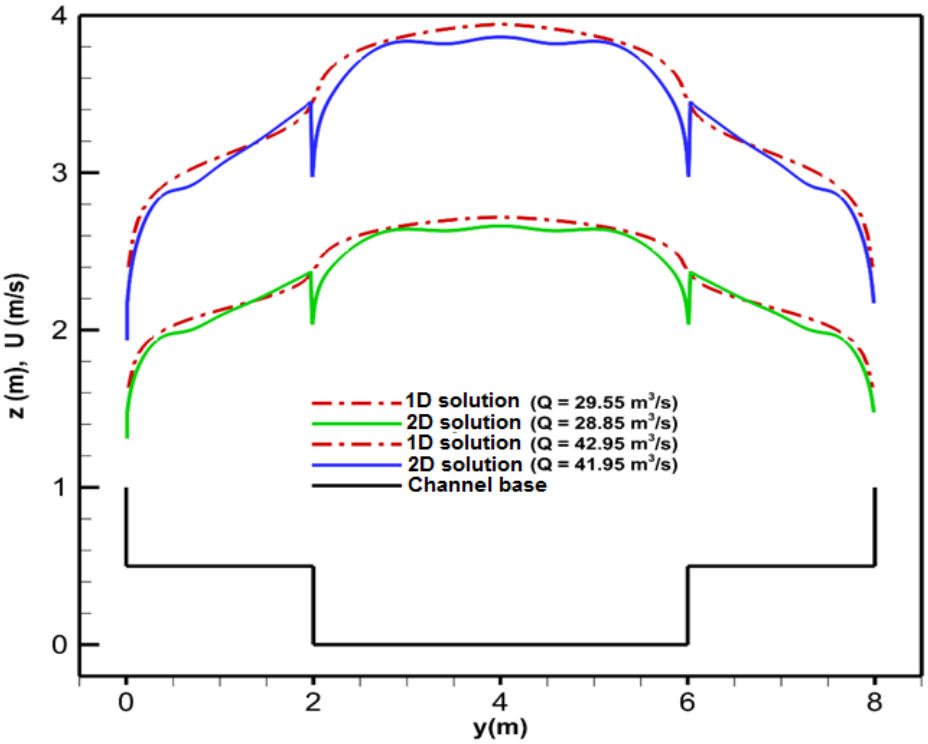

Figure 12. The comparison of depth-averaged velocities obtained from 1D SWE and 2D solutions

The SWE used in this study can be simplified for uniform flow. In this case all x-dependent terms will be dropped. Only the transverse variation of the velocity in the main flow direction, *u(y)* will be computed. The stress expression in Equation (4) is simplified for 1D flow.

$$\tau_{x,y} = (\nu + \nu_t)(\frac{\partial u}{\partial y}) \tag{9}$$

where the turbulent viscosity is described as

$$\nu_t = l_m^2(\frac{\partial u}{\partial y}) \tag{10}$$

Here, l_m is firstly computed in the channel cross section as described in [18] then averaged vertically from the base up to the water surface. In other words, l_m is the depth integrated turbulence mixing length.

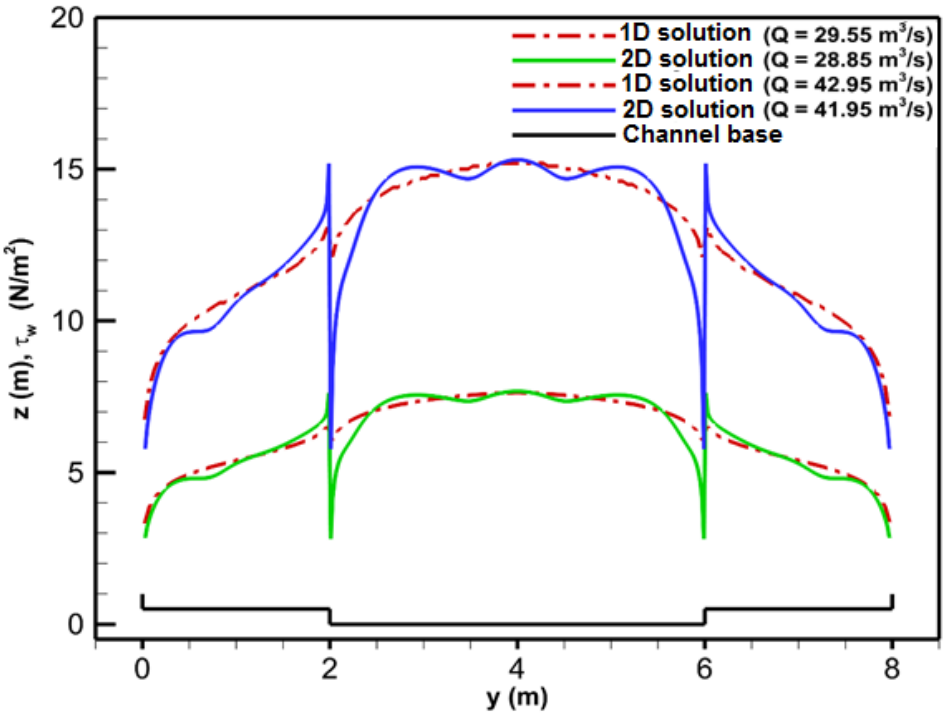

Figure 13. Comparison of wall stresses obtained from 1D SWE and 2D solutions

For a uniform flow in a compound channel, the 1D SWE results within 2D numerical solution results are presented in Figures 12 and 13. In 2D solution the 3-momentum equations are solved for the 3-velocity components without any simplification, and the secondary flows are also represented as they are. In Figure 12, the computed depth-averaged velocity distributions for two different slopes is shown within the channel cross section. The continuous lines show the 2D solution while the dashed lines show 1D solution. The computed discharge values for both of the slopes are also shown on the figure. In this comparison the difference between the discharges of 1D SWE and 2D solutions is less than 2 % without any calibration. A better fit can be obtained if some friction parameters are calibrated by using experimental data. For the same flow conditions, the comparison of computed wall stresses is illustrated in Figure 13. It is seen that the 1D solution gives quite accurate predictions for the wall shear stresses.

4. CONCLUSIONS

In this paper, the numerical solution of SWE is obtained for three different flow cases and results are evaluated to discuss validity and reliability of SWE as a mathematical model. The SWE with its hyperbolic characteristic, allow discontinuous solutions in the flow parameters. The capability of the numerical method in this sense is observed by solution of the supercritical flow passing around an obstruction in a channel as the first test case. The

stationary waves after the obstruction and the hydraulic jump before the obstruction are computed as examples of surface discontinuity.

The fundamental condition for validity of the SWE is that the horizontal dimension of the flow domain should be larger enough (5~6 times) than the vertical dimension, the flow depth. Since the momentum equation in the vertical direction is eliminated by assuming zero acceleration in that direction, hydrostatic pressure distribution is accepted. Thus, when the flow around an obstruction is studied with SWE, it should be recognized that pressure forces and thus the total drag force may not be computed accurately. Actually the primary outcome expected from the SWE solutions is the water depth. If the water depth is computed with sufficient accuracy, the depth-averaged velocities will also be obtained at the same level of accuracy. But, as in the second example, the flow passing through the sequential obstructions, inaccuracy in depth may accumulate due to complicated 3-dimensional flow features.

As the third example, in the uniform flow solution in a compound cross sectional channel, a fairly simple turbulence model is used. A turbulence mixing-length, that computes the weighted distances from an interior point to the walls, is sufficient to obtain accurate depth averaged velocity profiles. This conclusion indicates that satisfactory turbulence models can also be developed for 2D SWE formulations.

References

[1] Toro, E.F., Shock-Capturing Methods for Free-Surface Shallow Flows, Chichester. John Wiley & Sons, 2001.

[2] Toro, E.F., Riemann Solvers and Numerical Methods for Fluid Dynamics. A Practical Introduction, Berlin, Heidelberg. Springer-Verlag, 2009.

[3] İşcen, B. N., Computer Code Development for Numerical Solution of Depth Integrated Shallow Water Equations to Study Flood Waves, Yüksek Lisans Tezi, Orta Doğu Teknik Üniversitesi, Ankara, Türkiye, 2015.

[4] Alcrudo, F. and Garcia-Navarro, P., A High-Resolution Godunov Type Scheme in Finite Volumes for the 2D Shallow Water Equations, International Journal for Numerical Methods in Fluids, 16, 489-505, 1993.

[5] Roe, P. L., Approximate Riemann Solvers, Parameter Vectors, and Difference Schemes, Journal of Computational Physics, 43, 357–372, 1981.

[6] Versteeg, H. K., Malalasekera, W., An Introduction to Computational Fluid Dynamics - The Finite Volume Method, Pearson. Prentice Hall, 2007.

[7] Stoker, J. J., Water Waves, the Mathematical Theory with Applications, London. Wiley, 1957.

[8] Wu, C., Huang, G., and Zheng, Y., Theoretical Solution of Dam Break Shock Wave, Journal of Hydraulic Engineering, 125(11), 1210–1215, 1999.

[9] Zoppou, C. and Roberts, S., Explicit Schemes for Dam-Break Simulations, Journal of Hydraulic Engineering, 129(1), 11–34, 2003.

[10] Brufau, P. and Garcia-Navarro, P., Two-Dimensional Dam Break Flow Simulation, International Journal for Numerical Methods in Fluids, 33, 35–57, 2000.

[11] Yılmaz, B., Development and Validation of Two-Dimensional Depth-Averaged Free Surface Flow Solver, Yüksek Lisans Tezi, Orta Doğu Teknik Üniversitesi, Ankara, Türkiye, 2003.

[12] Canelas, R., Murillo, J. and Ferreira, R., Two-Dimensional Depth-Averaged Modelling of Dam-Break Flows Over Mobile Beds, Journal of Hydraulic Research, 51(4), 392–407, 2013.

[13] Raisee, M., Jafari, A., Babaei, H. and Iacovides, H., Two-Dimensional Prediction of Time Dependent Turbulent Flow Around a Square Cylinder Confined in a Channel, International Journal for Numerical Methods in Fluids, 62, 1232–1263, 2010.

[14] Wu, W., Sanchez, A. and Zhang, M., An Implicit 2-D Shallow Water Flow Model on Unstructured Quadtree Rectangular Mesh, Journal of Coastal Research, 59, 15-26, 2011.

[15] Wu, W., Wang, P. and Chiba, N., Comparison of Five Depth-Averaged 2-D Turbulence Models for River Flows, Archives of Hydro-Engineering and Environmental Mechanics, 51(2), 183-200, 2004.

[16] Yu, C. and Duan, J., Two-Dimensional Depth-Averaged Finite Volume Model for Unsteady Turbulent Flow, Journal of Hydraulic Research, 50(6), 599–611, 2012.

[17] Fe, J., Navarrina, F., Puertas, J., Vellando, P. and Ruiz, D., Experimental Validation of Two Depth-Averaged Turbulence Models, International Journal for Numerical Methods in Fluids, 60, 177–202, 2009.

[18] Aydın, İ., Nonlinear Mixing Length Model for Prediction of Secondary Currents in Uniform Channel Flows. Journal of Hydraulic Engineering, 135(2), 146–153, 2009.